PROCEEDINGS, 49th Workshop on Geothermal Reservoir Engineering
Stanford University, Stanford, California, February 12-14, 2024
SGP-TR-227

Geothermal Reservoir Simulation Workflow for a Low-Enthalpy Fracture Hosted Resource

Tim Salter[1], Ehsaan Nasir[1], Colleen Barton[1], Ayman Samy[1], Christopher Harper[1], Hector Andrade[1], Peter Vivian-Neal[2,]
Peter Harrison[2]

[1]Baker Hughes Reservoir Technology Services, Houston TX, USA 77073, [2]Kalahari Geo Energy LTD, Lusaka, Zambia

tim.salter@bakerhughes.com

Keywords: Dynamic Reservoir Modeling; Discrete Fracture Network Modeling; Fault-hosted Geothermal Reservoir

ABSTRACT

Completed at the request of Kalahari GeoEnergy, this study refines the resource estimate associated with the Bweengwa River geothermal resource in the Kafue Trough of Zambia. The productivity hosting fracture system present within the basement has been modelled using a discrete fracture network (DFN) with input derived from core review and the faults contained within a newly derived fault framework. Deterministic faults and stochastically generated fractures sets of the DFN were utilized to perform an integrated modelling workflow and deliver 3D models with predictive resource capability. The DFN fracture model was conditioned to well test transmissivities and calibrated to the thermal model and reservoir rock-type. The resulting parameters include directional hydraulic conductivity tensor and fracture porosity that were upscaled to provide input to dynamic reservoir fluid flow simulation.

A review of the composition of sampled fluids, alongside isotope ratios and interpreted downhole conditions suggests that primarily the geothermal water is derived from a meteoric source which has percolated from surface through permeable and fracture mediated processes, into the basement, where it is heated and subsequently driven upwards by convection. The integration of static parameters with the dynamic transmissivity enabled a confident initialization of the static model for simulation. Natural State Thermal equilibration runs showed stability of the thermal plume, maintaining a suitable balance of conductive and convective heat flow processes dominating in the Karoo (Permian) age sedimentary cap-rock and the resource hosting metamorphic basement respectively.

Simulation of prediction cases with existing well doublets highlighted the risk of injection water breakthrough related to permeability anisotropy. Geothermal power output was maximined by injecting into the shallower basement layers whilst producing from the deeper, hotter basement layers. An optimised development scenario of 3 producers plus 3 injectors, with production targeting the deep, hot up-flow and using well rate constraints consistent with the well test derived flow rates of up to 25 kg/s, proved to deliver a stable thermal output of 22 MWt over a 20 year span.

The study has provided a fundamental shift in quantification of the resource that may be developed by following a robust fracture-centric characterisation of the basement – by way of a discrete fracture network (DFN) sub-model – that was tied to the productivity proven in those wells tested to date. Further flow testing of wells and especially of deepened well penetrations that will help prove the character of the assumed hotter (>130°C) resource that is expected deeper than some 1000m below ground level.

1. INTRODUCTION

Kalahari GeoEnergy is undertaking the development of a geothermal power generation project of a minimum of 10MW, with aims for up to 20MW, in the Bweengwa River area at the southern boundary of the Kafue Rift basin. The geothermal resource is represented at surface as a suite of hot springs clustered along the basin bounding faults, but developed in the subsurface as a deep circulating geothermal system associated the Karoo age basin-bounding faults.

The resource has been explored in detail over the last 11 years through a combination of geophysics, surface mapping, geochemical sampling and the data from twenty-one shallow boreholes (Figure 1). Several studies have been conducted by and on behalf of Kalahari to integrate the data and mature the underlying conceptual models based on newly acquired data and so assess the potential of this resource to provide the desired geothermal power. The recent deepening two existing slim wells has suggested the resource may locally be hotter than considered to date.

The existing available data, interpretations and prediction models have been reviewed and the underlying conceptual resource model has been updated to capture several elements not addressed in previous resource models. Specific focus was placed on updating the thermal model using newly acquired deepened well data and adding characterisation of the resource hosting basement. The productivity hosting fracture system present within the basement has been modelled using a discrete fracture network (DFN) with input derived from core review and the faults contained within a newly derived fault framework. An integrated modelling workflow was utilized to deliver 3D models with predictive resource capability.

The database comprised a combination of original datasets, historical interpretation documents and previous resource summary and estimation reports. The existing data sets, interpretations and models provided by Kalahari GeoEnergy provide significant characterisation of the Bweengwa resource. Together the database presents a wide ranging view of the resource area with particular depth in well data, summary 3D geomodels, water geochemistry, surface mapping and geophysics.

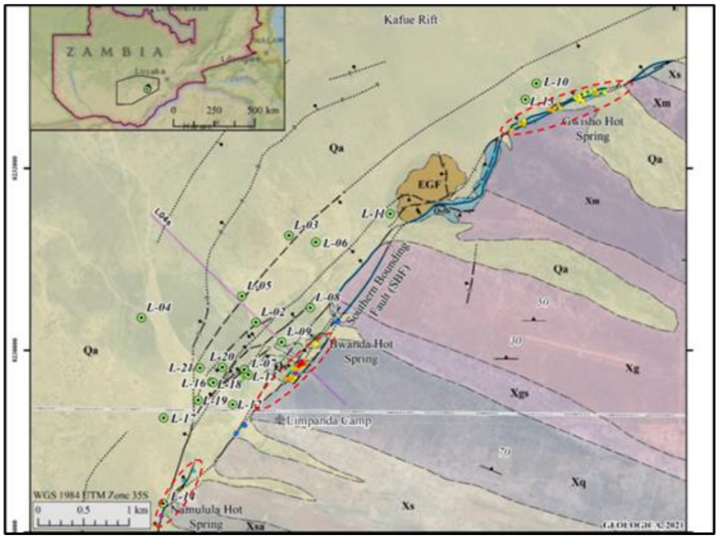

Figure 1. Summary surface geology map showing the Namulula, Bwanda and Gwisho hot springs plus the exploratory LOCH (L) wells focused on the Bweengwa resource (from Geologia Geothermal Group, 2021).

2. GEOMODEL BASE DATA

The geomodel was constructed to provide a balance between the very detailed data that is obtained locally (e.g. in core or well-logs) and the sparse data (e.g. remote sensed geophysical volumes) that is available for majority of the modelled volume of interest. For this study, the key aspects of the geomodel development were 1) revision and simplification of the fault framework; 2) simplification of the Karoo stratigraphic units and increased focus on the basement; 3) updating of the well-based temperature profiles and the associated 3D temperature model; and 4) revision of the basement permeability description through inclusion of a fracture characterisation.

In addition to refining the structural and stratigraphic framework of this site geomodel development included in depth assessment of core data, geophysical data, geochemistry and well test data to gain a better understanding of fluid sources and hydrogeology, required input for dynamic reservoir modeling.

2.1 Well Core Data

A total of 21 wells have been drilled within the study area. Most wells were drilled by a combination of rotary drilling from surface and subsequently coring to total depth (TD). This provides a wealth of cores that could be examined by way of the whole core photographs in which lithology, fracturing, internal structure and alteration could be viewed. The cores are not oriented (excepting LOCH-15 and LOCH-14 where well deviation allowed a high-side reference) but whenever the core was arranged in the core tray with maximum apparent dip across the tray this did allow the approximate dip of structural features to be noted (Figure 2).

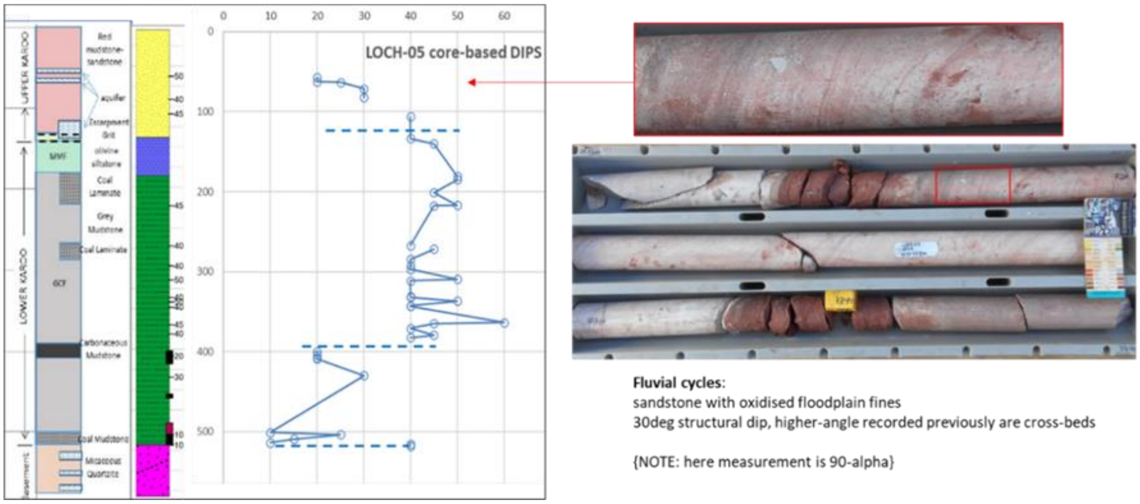

Fluvial cycles:
sandstone with oxidised floodplain fines
30deg structural dip, higher-angle recorded previously are cross-beds

{NOTE: here measurement is 90-alpha}

Figure 2. Example well data QC of photographs and newly derived dips against vintage lithology columns.

2.2 Geophysics Data Assessment

The geophysics datasets provided a comprehensive amount of geophysical exploration data including gravity, magnetics, radiometric, depth surfaces interpretation, satellite images, and interpreted faults polygons. 3D resistivity model was built based on the AMT (Audio-frequency Magnetotelluric) depth slices and the topography information (Figure 3). Subtle smoothing filtering was used to reduce the remaining interpolation numerical artifacts.

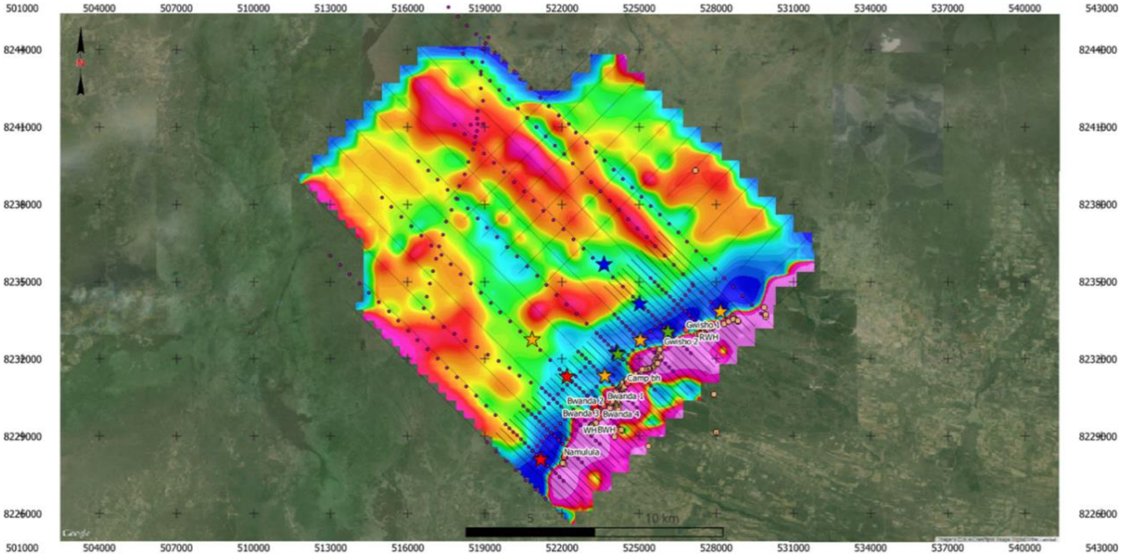

Figure 3. Consolidated QGis project with all relevant available data.

By applying to the 3D resistivity model the Thinned Fault Likelihood or TFL concept (Hale, 2013) we generated a property volume that highlights linearly consistent features that are interpreted as faults. The Thinned Fault Likelihood (TFL) attribute process automates computation of faults likelihood, determining fault geometry, fault extraction and the estimation of fault throw providing sharp fault traces on horizontal and vertical sections through the volume. Although this method was originally designed and implemented for seismic data, it can as easily be applied to other types of 3D geophysical data. Figure 4 shows its potential to aid interpretation of the fault model applied in this study by highlighting features correlatable with geological faults. Applying this method supports a reinterpretation of the fault model used in this study.

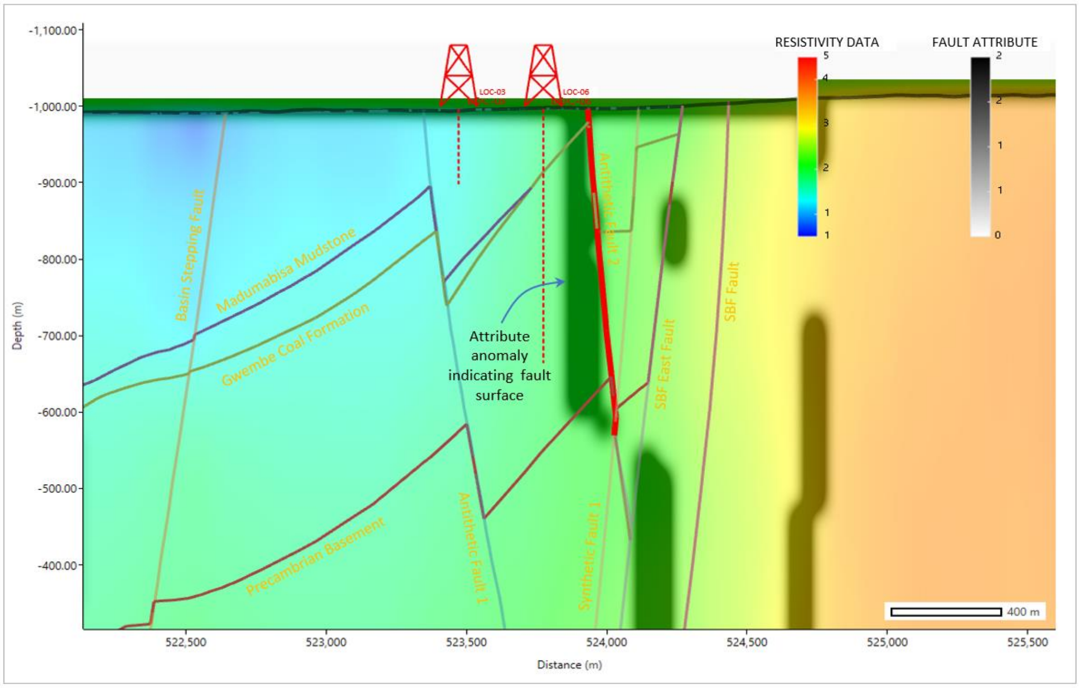

Figure 4. Thinned Fault Likelihood attribute feature delineation from the AMT resistivity volume.

2.3 Geochemical Data Assessment

Geochemical data was available from many of the LOCH wells in addition to samples from the Namulula, Bwanda and Gwisho hot springs that occur along the edge of the Kafue Trough. An examination of the water compositional and isotopic data for the Bweengwa River geothermal asset indicates that the geothermal fluid seen at surface springs is likely to be primarily sourced from meteoric water percolation, and fracture communication, down towards the basement where it is heated and subsequently rises due to convection. The faults within the basement are thought to be central to the occurrence of the hot brines near-surface at Bweengwa and must be associated with permeable fracture zones.

Using dissolved silica as a geothermometer suggests that reservoir/source temperatures will be 130° to 140°C minimum, based upon classical silica solubility curves at the calculated source water pH values. The conceptual model is thus one of downward percolating fluid gradually being heated by conduction of the hot country rock (e.g., at least 140°C at depth in excess of 1km below ground level and then, where faulting, stress and permeability allows, the hot fluid returns to shallower depths, migrating to surface (at hot springs) via faults and fractures in the basement.

The observations of magnetite in some wells, along with the reported sulphurous smell from some samples suggests that a significant proportion of the sulphate detected in waters may be oxidised sulphide since crystallisation of magnetite requires low to intermediate oxygen concentrations to be present. It is therefore considered that at downhole source conditions, H_2S and HS, rather than sulphate may be prevalent, and that an additional minor influx of oxygenated waters exist at shallower depth. This is further supported by the observation that at the downhole condition, if the attributed sulphur were sulphate the water would be self-scaling with respect to anhydrite (CaSO4). Observations of gypsum veins in the upper Karoo and gypsum being mined regionally support this supposition of a shallower influx of sulphate bearing, at least partially oxygenated water, this being a deposit typically found at temperatures below 42°C in the presence of sulphur and oxygen. Deeper water may therefore be sulphide bearing hotter waters and shallower waters sulphate bearing partially oxygenated cooler waters. The shallower influx of oxygenated water, although likely to be only in low quantities, would be sufficient to oxidize sulphide to sulphate on mixing.

2.4 Productivity and Injection Assessment

We investigated well test data conducted on wells LOCH-18, LOCH-19, LOCH-20 and LOCH-21 in 2020 and 2021 as well as the most recent well test for well LOCH-5 conducted in 2023. Well tests were conducted through slotted liner intervals between the Lower Karoo and basement lithologies. Well test durations varied among the wells between 5 and 20 days to model reservoir deliverability and testing data showed stable production rates. Well injectivity was modeled to define the maximum injection capacity for each well.

Table 1 shows a summary of well performance modelling results including flow rates, Kh (permeability x thickness) values, possible zone of contribution, possible depth of feedzone, reservoir permeability and productivity index. The wells can be ranked as shown, LOCH-18 is the highest productivity, LOCH-21 is medium, wells LOCH-20 and LOCH-19 are low and well LOCH-05 is very low. Figure 5 shows a schematic that includes the five well tests, the basement zone penetrated, and the possible contribution zone for each well.

Table 1. LOCH well productivity summary

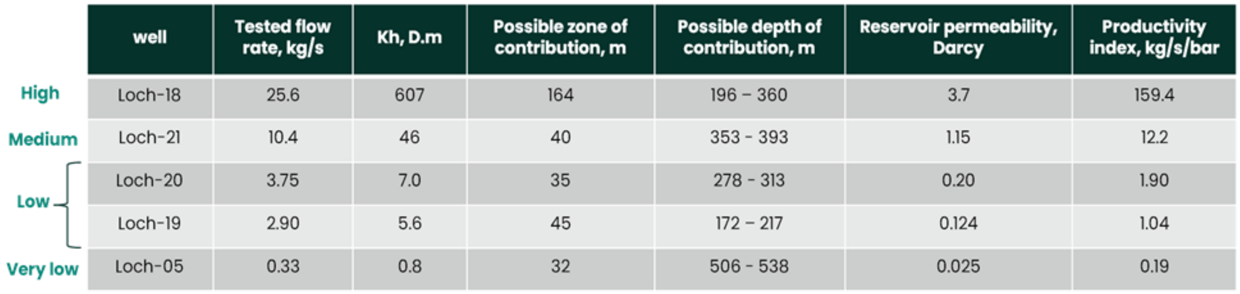

	well	Tested flow rate, kg/s	Kh, D.m	Possible zone of contribution, m	Possible depth of contribution, m	Reservoir permeability, Darcy	Productivity index, kg/s/bar
High	Loch-18	25.6	607	164	196 – 360	3.7	159.4
Medium	Loch-21	10.4	46	40	353 - 393	1.15	12.2
Low	Loch-20	3.75	7.0	35	278 – 313	0.20	1.90
	Loch-19	2.90	5.6	45	172 – 217	0.124	1.04
Very low	Loch-05	0.33	0.8	32	506 - 538	0.025	0.19

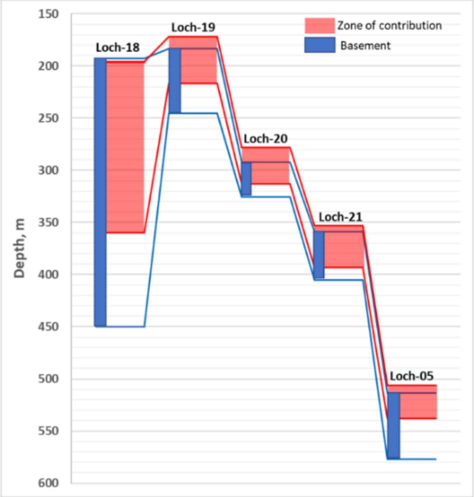

Figure 5. Basement and possible zones of contribution schematic based on well test analyses.

3. GEOMODEL BUILD

3.1 Model Setup

One major consideration for building the geomodel was the size of the grid to be built from the initial geological framework – as a regular grid is required for on-pass to the numerical simulator. It is normal to scale the grid against input data and modeled features. In this study as the wells are the key input it was important to ensure all such well data could be suitably honoured.

A grid of 50m x 50m laterally was chosen as suitable to capture a representation of the subsurface. This allowed for important individual wells such as LOCH-18, LOCH-19, LOCH-20 and LOCH-21, which are only separated by as little as 250m to each be fully captured in the model without being overprinted by or unnecessarily averaged with each other. In the case of redrilled wells (e.g., LOCH-16 and its re-drill as LOCH-18) only the more informative of these two wells was loaded to the model as this contained all of the information that was also available from the less informative wellbore.

3.2 Stratigraphic Framework

Reference to the lithological descriptions from the LOCH wells confirms that of those wells penetrating the basement two or three main lithologies may be identified. In the case of this review, all lithologies were checked from the available core photographs and QCd against additional drilling reports.

Comparing the basement lithologies encountered in several wells with the basement exposures (Figure 6) confirms that as a minimum it is possible to extrapolate the quartzite and schist dominated assemblages beneath the Karroo.

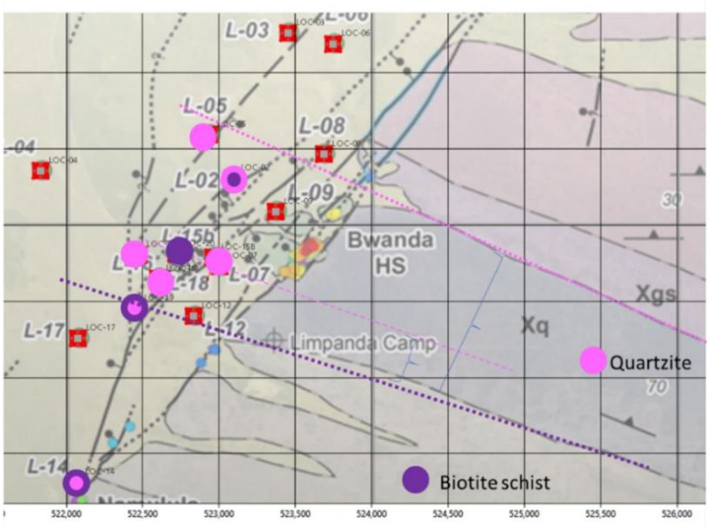

Figure 6. Pre-Karoo lithologies observed in existing LOCH wells follow the primary division of the basement noted in outcrop to the SE, with WNW striking and NNE dipping quartzites dominated rocks overlying schist dominated rocks.

The most important Karoo subdivision is between the (Lower Karoo) mudstones and the Upper Karoo sandstone rich Escarpment Grit Formation (EGF). Drilling results have identified cool water inflows (from riverine or artesian ground-water systems) associated with these sediments and in the LOCH-3 and LOCH-6 wells such inflow, close to the base of the EGF, caused notable drilling issues. The contact between the EGF and the Lower Karoo is an angular unconformity and the Madumabisa thins towards the Southern Boundary Fault (SBF) and the margin of the Kafue trough below this unconformity. This results in the EGF overstepping onto the Basement. This issue causes the most complications in the correlation.

From this assessment, the stratigraphic framework adopted in the model simplified the sediment cover into three main packages, the Lower Karoo, the Upper Karoo and then a thin Tertiary alluvial cover. This was countered by adding detail to the basement through the division into quartzite dominated sub-crop that overlies a conformable but deeper biotite schist dominated interval (Figure 7).

The top surface of the geology grid was provided by a digital elevation model of the present day ground surface was exported from the previous model and imported into the model with a point spacing of 10 x 10 m laterally to ensure accurate representation of the ground datum.

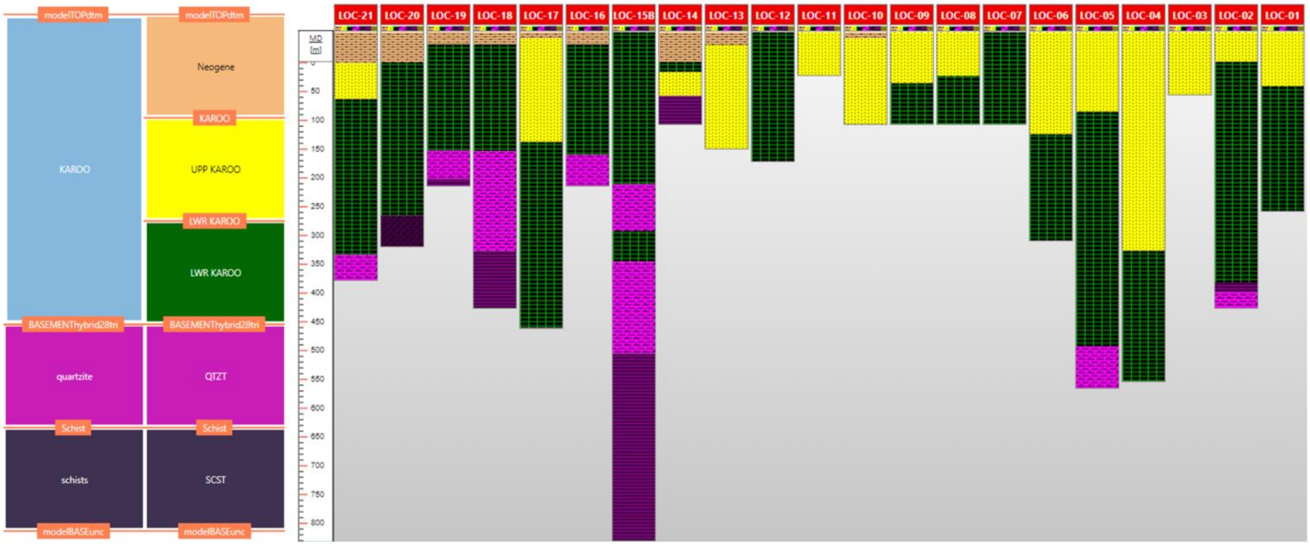

Figure 7. The stratigraphic framework of the geological model compared to lithology logs. The top of basement and top of Lower Karoo are the primary internal reference horizons.

3.3 Basement Mapping

The basement structure has been derived from a combination of mapping stratigraphic tops and introducing faults where data supported this. A first pass mapping of the top basement shows that although the SBF is a major feature laterally and obviously has long-lived significance, its current vertical throw required to match well tops is not significantly in excess of other faults that are needed (can be introduced) to account for top basement topography within the basin north-west of the SBF. It is observed that the elevation difference from LOCH-19 to LOCH-17 and likewise LOCH-18 and LOCH-21 suggests a significant down-to-basin fault with up to 200 metres of displacement (Figure 8).

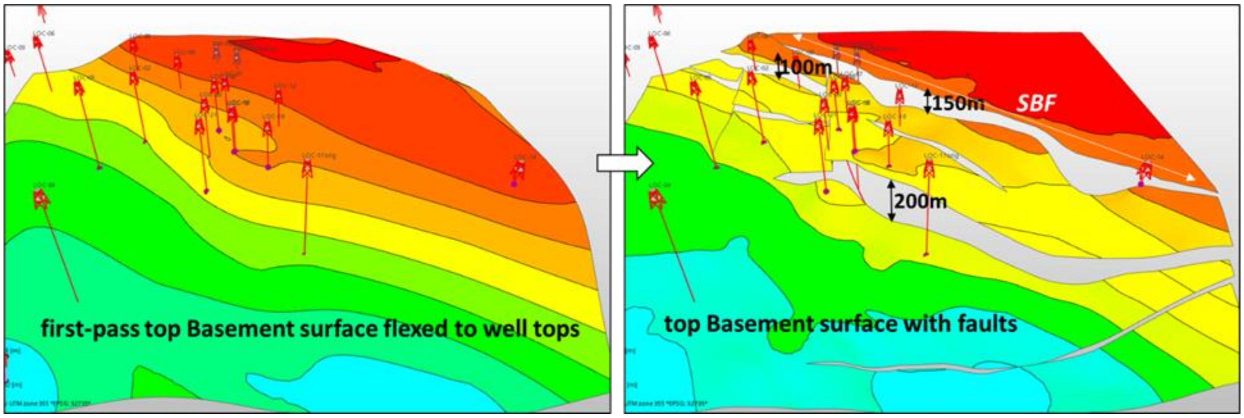

Figure 8. Eastward looking perspective of the top basement surface suggesting greatest fault displacements may lie basinwards of the SBF bounding fault.

For those wells that did not penetrate the basement, limited estimates of the depth (from well TD) to the basement could be attempted for some, dependent upon the stratigraphy and/or temperature noted towards the base of the drilled section. In addition to the top basement unconformity horizon, it was considered important to introduce an approximate intra-basement top schist horizon to provide a primary delineation of rock types for subsequent fracture and thermal property modelling. None of the LOC wells have proven the total thickness of quartzites (e.g. where the overlying gneisses are still preserved at subcrop to the top basement) within the Kafue Trough. Control on the total thickness of the quartzites was therefore estimated from the width of the adjacent (in the footwall to the SBF) mapped surface outcrop. There is no remote sensing/geophysical determination of the quartzite-schist contact, so instead this horizon was created from geometric considerations, creating a north-easterly dipping surface aligned with the regional strike of the basement shear zone and then tying it to the available well data. The process for constructing the intra-basement top schist depth horizon is summarized in Figure 9.

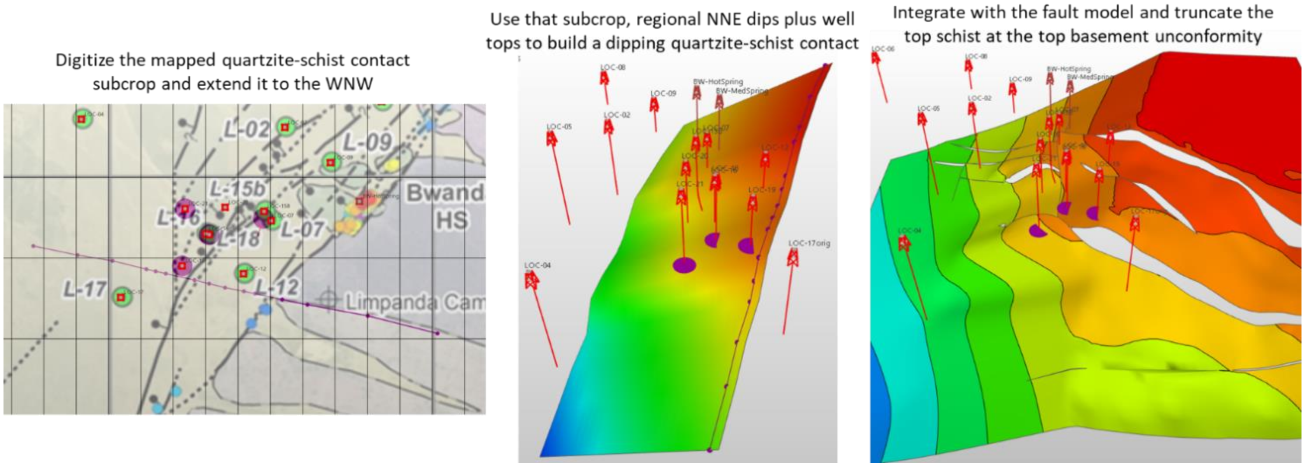

Figure 9. The process for constructing the intra-basement top schist depth horizon.

3.4 Fault Framework

Faults and their expression within the basement are central to the definition of the geothermal resource under investigation here. The structural framework adopted here has faults that pass with continuity from the basement to the cover (Karoo plus Tertiary sediments). This indicates an underlying concept that although major faults (e.g. the bounding SBF) may have moved prior to Karoo deposition, but all faults remained active or have been reactivated significantly after Karoo times. Notably, the presence of an unconformity between the Lower and Upper Karoo (seen regionally in overstepping of the Upper Karoo and additionally proven in the well data of this study by difference in structural dip domains) confirms that fault movement continued through Karoo times.

A well based data review of the previously modeled faults was conducted for several wells to sense check the faults contained in the 3D model. For most faults reviewed there was typically no strong justification for a fault at that particular depth (as extracted from the previous model) in the core, although often some evidence could be found in the sections 10-20m above or below the model fault (as per examples in Figure 10). It is important to note that most wells, especially in the cored basement quartzite sections contained several indications (brecciation, cross-cutting fracture fills) of possible large scale faults at many depths, but for none of these – due to lack of a more detailed intra-quartzite stratigraphy, was the relative magnitude of displacement quantifiable. The logical conclusion is thus that the basement comprises more faults than have been modelled to date. It is thus considered that most existing model faults have uncertainty in how they are carried forward or even required in a new model framework. Review of deepest well LOC-15 faults from the core photographs has, however, confirmed the previously interpreted basement repeat, duplicating some 70m of drilled section.

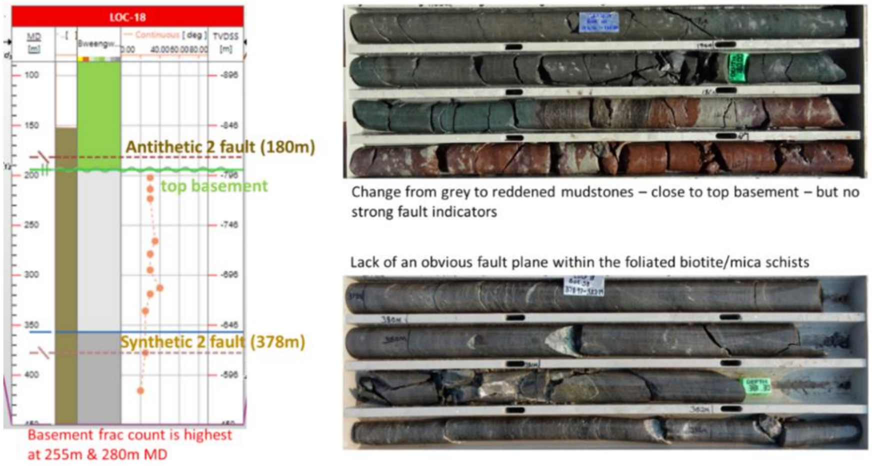

Change from grey to reddened mudstones – close to top basement – but no strong fault indicators

Lack of an obvious fault plane within the foliated biotite/mica schists

Figure 10. Review of antithetic and synthetic model fault-cuts on LOCH-18.

As a final investigation into the structural framework of the Bweengwa resource the structural dips recorded from core were compared by geological unit across the wells where such data allowed (Figure 11). The dips have no respective azimuth (as cores are not oriented) but do allow for lateral and vertical changes or trends to be investigated. This analysis implies that the LOCHH-21 should be separated by a major fault from the other nearby wells (LOCH-18, 19, 20 etc.) that can be considered to have been accompanied by fault block differential rotation.

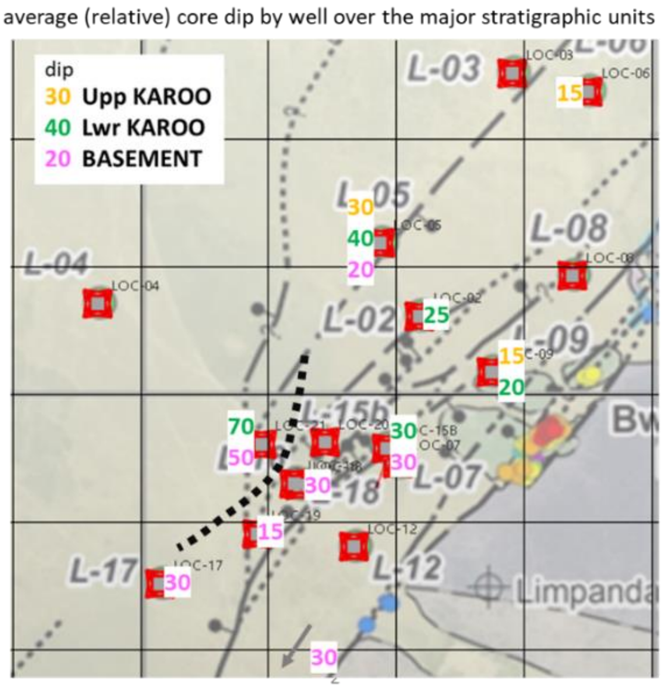

Figure 11. Synthesis of structural dip estimated from core photographs for the main geological units.

the next most significant consideration was the need for a major basin-wards stepping fault separating LOCH-21 and LOCH-17 from other wells further east. The location of this fault was guided by reference to the fault likelihood volume (derived from the MT data) that identified an apparent lineament through the 300m – 800m below ground level depth range (Figure 12).

Further faults were introduced to match other minor lineaments and give the requisite overall down to the basin displacement of the basement as well as the reverse fault explicitly required to tie LOCH-15. The final framework was constructed using surface fault intersection lines and applying suitable dip values to match well tops (e.g. LOCH-15) or MT lineaments at depth, with iteration used to ensure a suitable overall match.

The geomodeling software utilized in this 3D model build has full flexibility to match and capture accurate intersections between both planar and non-planar faults, but where possible the fault were kept relatively smooth as describing a similar fault relay system.

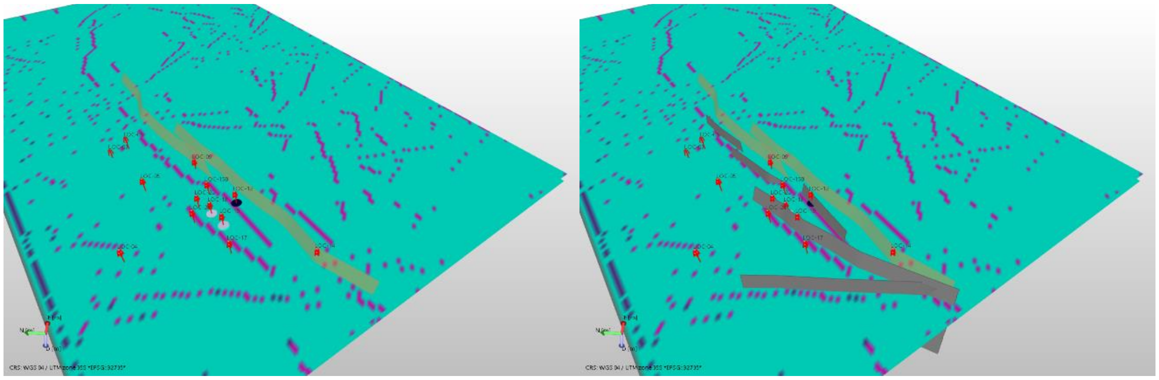

Figure 12. Lineaments used to position faults in the basin margin. The basin bounding faults (SBF) mappable at surface (dark orange) are not well imaged, however, the lineaments can be used to position the down to the West faults that control deepening of the basement under the Karoo.

Plan view of the faults at basement level (Figure 13) shows the overall basinwards stepping of the top basement surface so that it reaches a depth approximately 670m below ground level beneath the collar of LOCH-04. Fault heave (horizontal displacement) gaps are relatively narrow as a result of the steep (70+ degrees) fault dips modelled. The exception to this is the E-W reverse fault in LOCH-15 where a dip angle of 50 degrees was used (still possibly too steep for a reverse fault) to match the fault cut and also not create additional complexity in the adjacent LOCH-20 well.

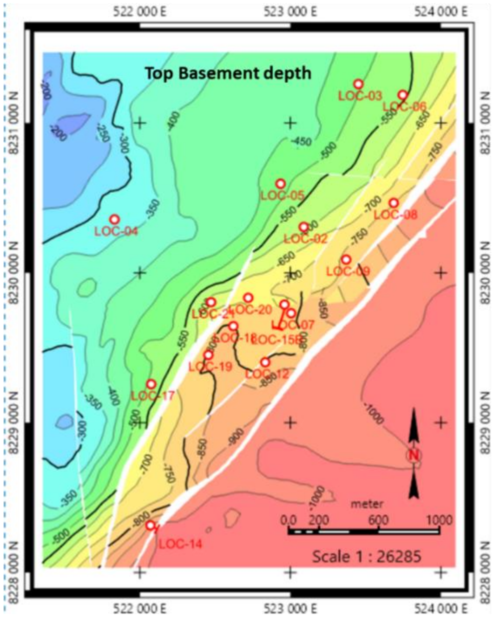

Figure 13. Top Basement depth horizons after inclusion of the 3D fault model.

Convective heat-flow up one or more of the intra-basial faults and their immediate damage zones within the basement is supported as the geothermal gradients from the basement sections of the hottest wells (e.g. LOCH-18) are representative of convective heat transfer. Within the sedimentary cover (with the exception of the lowermost Karoo that may be fractured in some wells) a conductive heat transfer regime is indicated. Thickness changes support extension of the faults from the basement into the Karoo, but once above the lowermost Karoo these faults are also considered to be hydraulically tight.

3.5 Temperature Model

Subsurface temperature data was provided by way of direct measurements from the sequentially drilled shallow wellbores and also by indirect inference based upon surface geothermal expressions, soil temperatures and fluid geothermometry datasets. The most important dataset comprised the temperature versus depth logged profiles and maximum bottom hole temperatures recorded from well logs. Each well typically had more than one temperature log, representing different logging runs and the variability between each such run often illustrates the perturbation of the wellbore environment during drilling, logging and well testing as the normally 'static' downhole environment is affected by introduced fluids and well hardware.

The suite of temperature profiles previously analyzed were reviewed to confirm that they were representative and consistent. Eight (8) of the 21 LOCH wells required some modification of the temperature versus depth profile (examples are shown Figure 14).

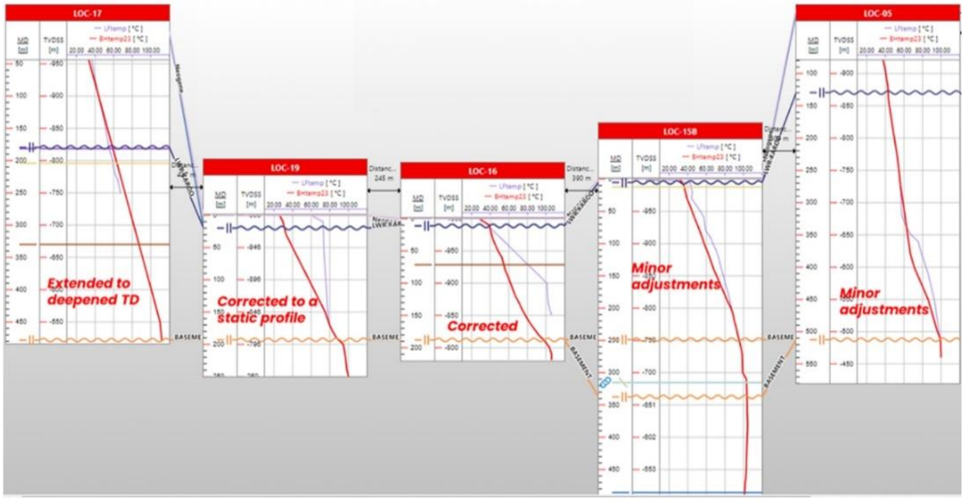

Figure 14. Examples of the corrections applied to the well-by-well stabilized temperature profiles used as the starting point for the 3D temperature model.

The 3D temperature model for Bweengwa is applied as a property within the geological grid. Validation of the MT resistivity volume and its derived geological elements (such as base of the low resistivity clay-cap) has shown that this is a variable match to well data and the well data itself has been considered as the most important input to the 3D geological model. The temperature model for this study was built from an initial 3D temperature grid using the NE-SW aligned intra-basin faults (and their expected permeable damage zones that allow convective upflow) as guides to the elongation/alignment of the temperature field. Isotherm surfaces from the previous model were then introduced and referenced to understand where the new temperature model was showing most deviation. Control pseudo wells were introduced iteratively around the LOCH well penetrations. The expected temperature profile was constructed for each pseudo well, honoring the position of the top basement and its location within (e.g., as LOCH-18) or peripheral (e.g. as LOCH-04) to the main heat plume.

The temperature model was built twice. Firstly, as part of the initial suite of property modelling and then again after initial equilibration runs of the dynamic model suggested hotter temperatures were required in the core of the plume at the base of the model to honor the temperature data. The final temperature model has a maximum temperature of 140°C at the base of the model. Laterally at the edges of the plume the temperature degrades slowly to approach lower in-situ values more comparable to those expected where geothermal upflow does not occur. The lateral gradient of this degradation is in the order of 50 - 100°C/km.

3.6 Fracture Analysis

No single fracture characterisation was available within the database, but individual wells contained fracture information from the various core reporting schemes. This included descriptive reference to fractures, veins and associated mineralization/hydrothermal features, depth tabulation of individual structural features (foliation, veins, bedding and fractures) and an alternate indication of the open/uncemented fracture intensity form the RQD (rock quality) measurements. All of these descriptive references could be cross-referenced back to the supplied core photographs.

The RQD logs were used to derive equivalent fracture/m counts and these were plotted for wells to investigate any relationships to lithology, location and depth below basement (Figure 15). This suggested an average fracture intensity of around 1/m overall but increasing to 3-4/m in local (up to 5m thick) concentrations.

The flow of many tested wells had come from the 20m-30m interval below top basement, suggesting that this was the most fractured. This initial data review would suggest that actual fracture counts derived here do not support that assumption. Wells such as LOCH-5 (Figure 16) and LOCH-21 may in fact show an increase in fracturing below the first 30m of basement depth. These counts, however, do not reference any estimated or proven flow potential. More deep penetrations with flow profiles taken across the basement will help to confirm the role of the uppermost 20-30m vs deeper faults in controlling the hot fluid outflow.

Following the initial data review and highlighting of the poor fracture characterisation, KGE performed a further core data review across the available cored sections. This provided a more consistent suite of fracture logs that were suitable for input into the later (DFN) fracture model.

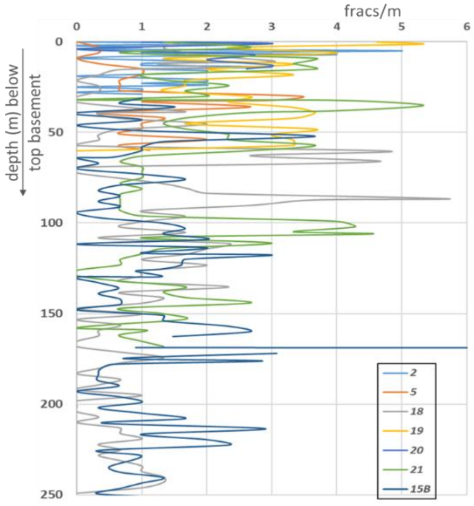

Figure 15. Comparison of fracture intensity curves derived from the RQD data – plotted to a common datum at top basement.

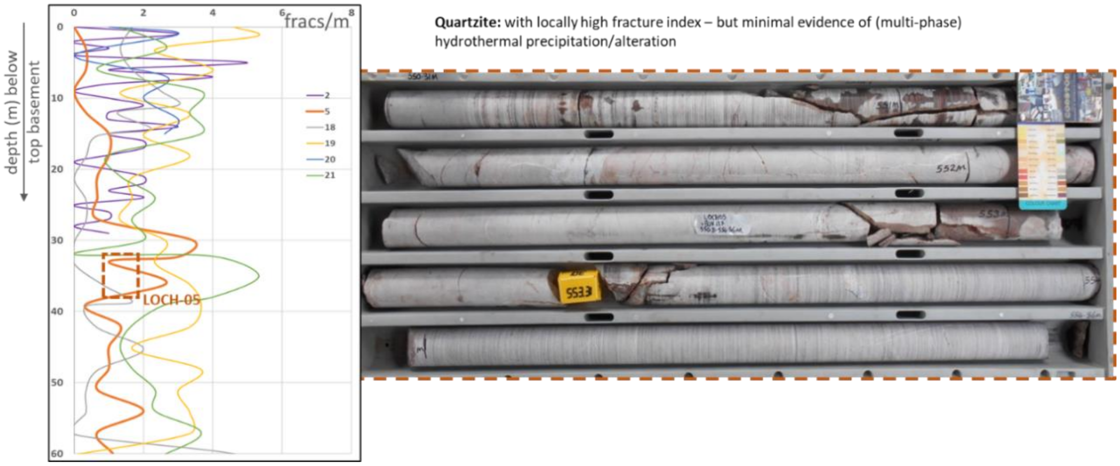

Figure 16. Detail of the LOCH-5 core and fracture count 30m below base Karoo.

4. DFN MODELLING

4.1 DFN Fracture Conceptual Model

The fracture conceptual model is comprised of large scale hydro-structures (faults) that can be described deterministically, and smaller scale structures that are only partially observed in wells, or not at all between wells, and are described stochastically. The hydro-structural model is interpreted from the structural Fault Framework model as described above. The model is augmented by more direct observation of fluid production in wells.

Smaller scale structures are observed in terms of their presence in well based core data that provide interpreted statistics of their spatial occurrence, intensity, and dip. Indications of their effects on fluid flow can be examined through the correlation of core fracture occurrence with anomalies in pressure and temperature gradients or spinner logs as well as drilling losses. Unoriented core from 17 wells were used to identify fracture dip, intensity and spatial occurrence (supplied by Kalahari Geo Energy LTD following the initial data review request). Orientations are important for understanding the alignments of fractures, as they control connectivity and anisotropy of the network of fractures beyond the wells, and the incident stress on the fracture planes determines their likely hydraulic and mechanical properties. In this study, without oriented core or wireline wellbore image logs, fracture orientation was treated stochastically. The intensity of fracturing determines whether fluids can percolate through a connected network of fractures and the directional permeability and accessible porosity of that network.

The distributions of fracture orientations were divided into five (5) sets (Figure 17b-f) consistent with nine (9) major faults trends (Figure 17a) of the structural model. Table 2 lists the 9 major reservoir faults geometries and Table 3 summarizes the stochastic fracture distribution used to generate the 5 fracture sets (combined in Figure 18). Fracture set dips are constrained both by the major faults trends and fracture dips measured from core.

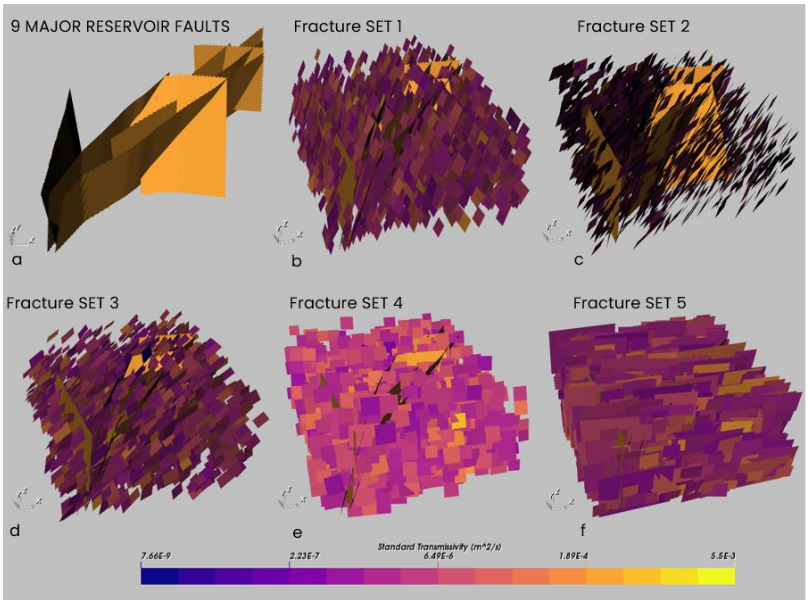

Figure 17. Deterministic faults and stochastically generated fractures sets of the DFN.

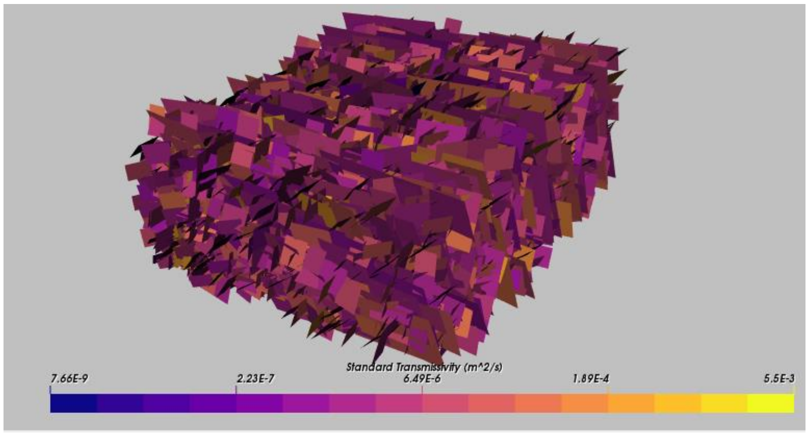

Figure 18. Final DFN realization utilized to calculate the contribution to reservoir permeability of the natural fracture and large-scale faults.

Table 2. Major Reservoir Faults Geometries

MAJOR RESERVOIR FAULTS			
Name	Trend	Dip	Length (m)
SPUR	N - S	85◦ W	1979
STRIKE2	NE - SW	75° W	3078
SBFsth	NE - SW	73° NW	4298
Strike1	NE - SW	80° W	1251
EW15	E - W	50° S	1742
Strike	NE -SW	85° W	1481
MagEW	E - W	85° S	1098
SBFnth	NE - SW	73° NW	3753
Strike3	NE - SW	85° W	1270

Table 3. Stochastic Fracture Distributions

DFN Fracture Sets				
Spatial distribution	Traingular: Generated in reservoir domain			
	Orientation: Bootstrapped from core			
Set 1	Strike	S_{mean} = 180°	S_{min} = 170°	S_{max} = 190°
	Dip	D_{mean} = 70°	D_{min} = 60°	D_{max} = 85°
Set 2	Strike	S_{mean} = 225°	S_{min} = 210°	S_{max} = 240°
	Dip	D_{mean} = 65°	D_{min} = 50°	D_{max} = 80°
Set 3	Strike	S_{mean} = 190°	S_{min} = 175°	S_{max} = 215°
	Dip	D_{mean} = 45°	D_{min} = 35°	D_{max} = 55°
Set 4	Strike	S_{mean} = 92°	S_{min} = 80°	S_{max} = 110°
	Dip	D_{mean} = 65°	D_{min} = 50°	D_{max} = 85°
Set 5	Strike	S_{mean} = 272°	S_{min} = 260°	S_{max} = 290°
	Dip	D_{mean} = 75°	D_{min} = 65°	D_{max} = 85°
Lengths	Power-law	Scaling exp=3.5	L_{min} = 50 m	L_{max} = 1500 m
Intensity	P_{32} = 1.0 x $10^{-2.5}$ in model domain extent			

Although there may be variability in fracture intensity between and within wells, the relative importance of fracture sets varies between wells. Understanding of any systematic trends in this variability is important for extrapolating likely structural and hydraulic characteristics to support well planning.

Fracture intensities were compared with lithology and mechanical properties (density, porosity) to explore reservoir property relationships. It has been well documented that brittle rocks host higher fracture frequencies than more ductile rocks (Erdis, et al. 2015, and others). With this approach, the more brittle quartzites with low porosity tends to have the highest fracture intensity compared to the other more ductile lithologies with higher porosity. The developed conceptual model is that quartzite has the highest fracture intensity, schist has average intensity, and mudstone the lowest intensity. The fracture intensity in quartzite is 30% higher than that in mudstone (Figure 19a).

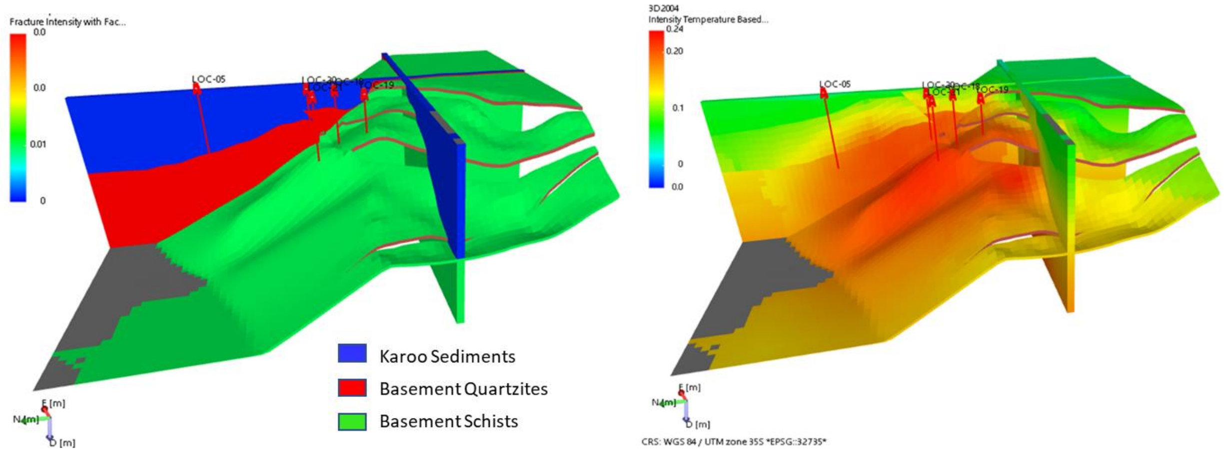

Figure 19 Within the Bweengwa study area a) fracture intensity driver based on primary rock types and b) Fracture intensity based on reservoir temperature.

Fracture intensity can also be correlated with reservoir temperature anomalies. Correlations of core derived fracture frequency with temperature gradient logs recorded over the cored intervals were inconclusive due primarily to the lack of overlap between recorded temperature logs and zones of core recovery. An alternate volumetric approach was applied using the temperature volume as a proxy for fracture intensity (Figure 19b). The final distribution of fracture intensity was derived by superposition of reservoir rock type and reservoir temperature based fracture intensities. An observed characteristic of the Bweengwa fracture system is that although fractures are widespread in the basement rock (in the 17 cored wells more than one fracture per meter was recorded on average) flow, as evidenced by production or anomalies in PT surveys and drilling information, is dominated by a small number of structures per well. This implies that flow is restricted to a sparse subset of fractures that lie within deformation zones that have sufficient intensity to form extensive interconnected networks.

Ideally such zones are identified from the image log interpretation where the local fracture intensity can verify the zones of high permeability. By further examining the predominant orientation of fractures within each deformation zone, one can infer the main trends of the likely fluid conducting structures and their relationship to lithology. Lack of image log data precludes this level of detail for this study, however, flow conducting deformation zones are assumed to define the zones of contribution of computed well permeability-thickness values used to

4.2 DFN Numerical Simulation

Numerical 3D DFN modeling is used to implement the interpreted conceptual model for natural fractures, quantify and test models for fracture parameters, and ultimately make predictions of likely structural and hydraulic properties in new areas of drilling. The finite element software used employs the hydrostructural approach of DFN model generation. This approach involves analysis and modeling which explicitly incorporates the geometry and properties of discrete features as a central component controlling flow and transport. In these DFN models, a stochastic 'pipe' network type algorithm is used to calculate the flow and transport through the fracture network.

The same base geomodel grid developed for structural and stratigraphic modeling was used to define the reservoir domain of the DFN. The modeling starts by interpreting the hydro-structural model, which is essentially the hydraulic companion to the interpreted geological structural model. Larger scale structures that may correspond to faults, or fault segments and can be associated with fluid conduits based on production information. These features generally form a deterministic skeleton for the description of fluid conducting fractures.

It is only possible to characterize some larger scale structures deterministically and only within the area where data is of sufficient quality and abundance. Between and beyond these structures a stochastic description of the fracture system is necessary based on the DFN conceptual model described above and the associated parameterization of fracture orientations, fracture intensity relative to 3D models for lithology and, if available, geomechanical properties. Expected variations in fracture orientation and intensity across the field are determined by the fracture characterization and association to the 3D geological model, but the locations, orientations and sizes of individual fractures are sampled by a stochastic approach.

In the absence of any direct means for determining fracture size distribution, a common interpretation is they follow fractal or multi-fractal scaling laws (King, 1983; Barton, 1992, Davy, 1993). The assumption is that fracture intensity-size follows a power-law distribution the exponent of which can be inferred by matching the intensity of fractures seen at the scale of the diameter of wellbores (decimeter) to the intensity-scaling implied by the fault model (kilometers) (Edris, et. al, 2015). It should be recognized that the intensity of open fractures is less than that of all fractures, due to sealing, mineralization and mechanics, and that intensity-size distributions for connected fractures can be quite different, as large fractures are more likely to form connected networks than small ones.

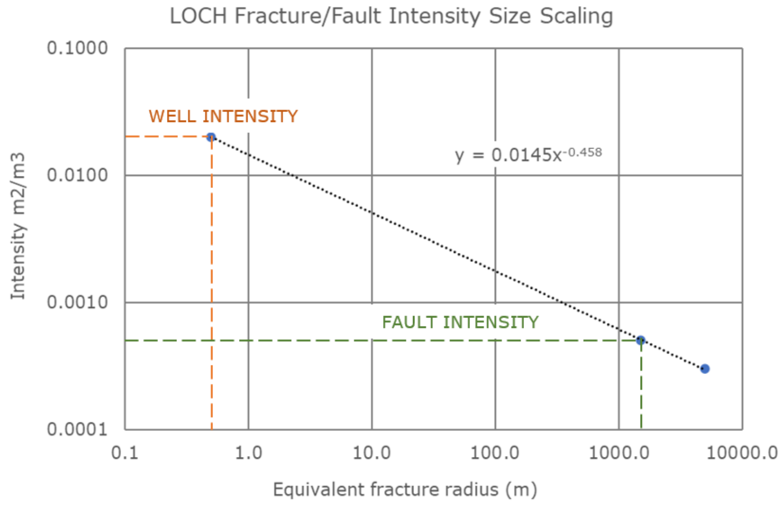

Figure 20. Fracture intensity-size scaling between well and fault scales.

Multiple realizations of the DFN were generated consist of the deterministic fault model and stochastic model of the fractures based on the conceptual models for fracture orientation, spatial distribution relative to 3D geological properties, and the power-law intensity-size scaling (Figure 20). An example DFN model is shown in Figure 18 total of 51973 fractures comprise the DFN sets of random fractures.

4.3 DFN Model Conditioning

As a test of the DFN model and to quantify uncertainty in hydraulic properties implied by the model around existing wells, multiple DFN realizations were generated and the computed permeability-thickness in each existing well compared to values interpreted from well tests (see Table 1). This DFN conditioning was limited to the kh analyzed from the well tests for each possible zones of contribution. The DFN results where these well-based measurements were matched to the deterministic and stochastically generated fractures that intersect each well indicate in the wells closest to the large-scale faults, and especially those with larger permeability-thickness, the deterministically specified faults are a significant part of the kh estimates from the model. In this simulation the matrix permeability is assumed to be negligible for DFN modeling.

Having inferred a DFN model from all available data to obtain geometric and dynamic fracture parameters down to the scale of those fractures seen in wells, the model can be used to simulate likely permeability encountered in wells. Although all relevant project data were used to develop and constrain the conceptual DFN model, uncertainty in the model could be reduced as new information is available to update and provide further model constraints. To evaluate the model and improve uncertainty, additional data on the location and properties of the connected fractures that control fluid flow in and around the wells from well based and core test data are recommended.

4.4 DFN Model Upscaling

The DFN concept is very useful since it naturally reflects the individual flow conduits in fractured rock, and the available field data. However, to model flow and transport on the regional-scale or over time it is necessary to consider larger-scale bulk properties in the context of an equivalent continuous porous medium (ECPM) continuum concept. To convert the properties of a network of discrete fractures of lengths less than the continuum grid blocks into ECPM grid properties, requires upscaling.

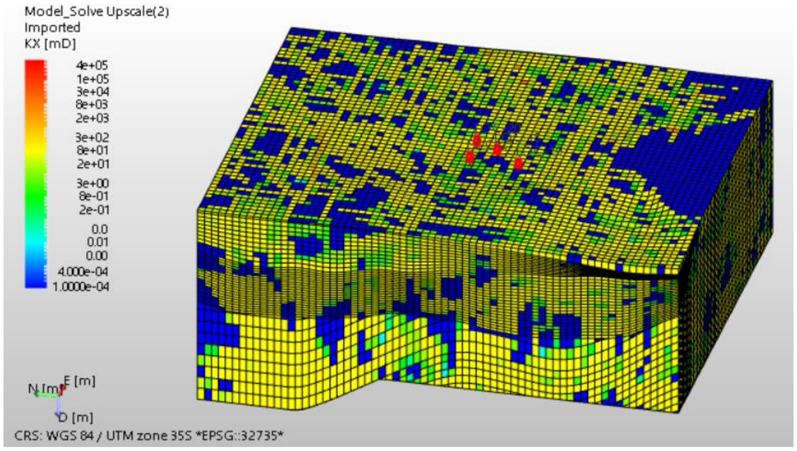

Figure 21. Upscaled DFN model used for reservoir dynamic simulation.

The resulting upscaled DFN realization parameters are a directional hydraulic conductivity tensor, fracture kinematic porosity and other transport properties (such as the fracture surface area per unit volume). A flux-based upscaling method is used that requires several flow calculations through a DFN model in different directions. In 3D, six directional components characterize the symmetric hydraulic conductivity tensor. Using the DFN flow simulations, the fluxes through each face of each grid cell are calculated for each head gradient direction. The hydraulic conductivity tensor is then derived by a least-squares fit to these flux responses for the fixed head gradients. This flow - based upscaling is accurate but can be computationally expensive.

Figure 21 presents the upscaled DFN volume and Figure 22 captures the derived K_x, K_y, and K_z permeabilities within the volume by filtering permeability below $3E^{-13}$ m^2.

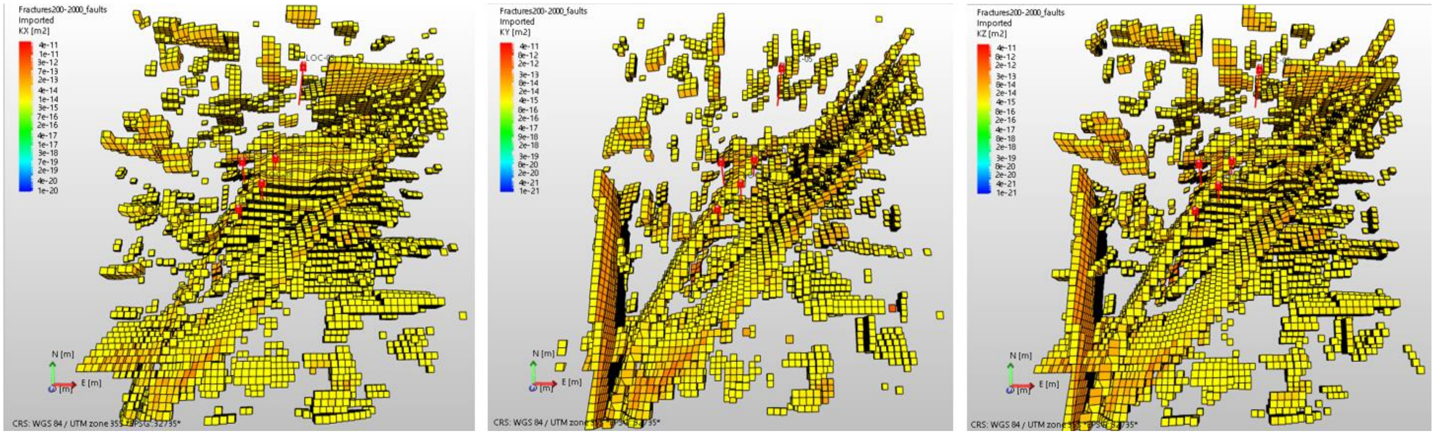

Figure 22. Derived K_x, K_y, and K_z permeabilities within the volume filtered below $3E^{-13}$ m^2.

5. DYNAMIC SIMULATION

5.1 Dynamic Model Properties

The 3D static geomodel grid with the upscaled permeability tensor was exported and incorporated into the dynamic simulation model. The grid was initially QCed to optimize dynamic modeling runs. The cell count in IJK (comparable to X, Y and Z) directions was 59 x

66 x 116 respectively. The total number of active grid cells was 188179 after setting cutoffs for cell thickness and volume to avoid numerical instabilities in simulations.

Four property volumes were uploaded to the dynamic model and modified for simulation requirements.

1. Zone IDs: were imported as is. The five zone IDs (Figure 23a) were defined to capture the main rock units: Sandstone layer 1 (Neogene sediments), 2) Sandstone layer 2 (Upper Karoo sediments), Mudstone layer (Lower Karoo), Basement quartzite layer, and Basement schist/undifferentiated layer.

2. Temperature – was QCed and a lower limit (i.e., surface temperature) was set to 25°C. The rest of the temp field was used as is (Figure 23b)

3. Porosity - poorly characterized from the datasets to date and was therefore estimated based upon knowledge of comparable rock types. The basement lithologies noted throughout the cored wells were largely compact with porosity associated only with occasional but often large fractures and vuggy core breaks, giving a very small overall volumetric porosity fraction. In keeping with typical fractured basement rock-types the quartzites and schists of zones 4-5 were assigned a 1% porosity. The mudstones of zone 3 were given a minimal 1% porosity, whilst the sandstone rich near surface zones 1 and 2 were assumed to have a 10% porosity (Figure 23c). The shallow, sandstone dominated zones (1 and 2) in red are 10% porosity and the deeper zones (3, 4 and 5) are 1% porosity.

4. Permeability – values in I, J and K directions were provided separately based on the DFN modeling (Figure 23d). Modifications were made to cells in the surface location of the Bwanda hot spring to connect it to the permeable basement just beneath. The horizontal permeability (I and J direction) for the mudstone layer was set to 2 mD and sandstone layers were assigned 20 mD. The vertical permeability for the sandstone and mudstone layers was set to 0.4 mD. This was to ensure the water produced at the surface was via the hot spring location as defined in the model.

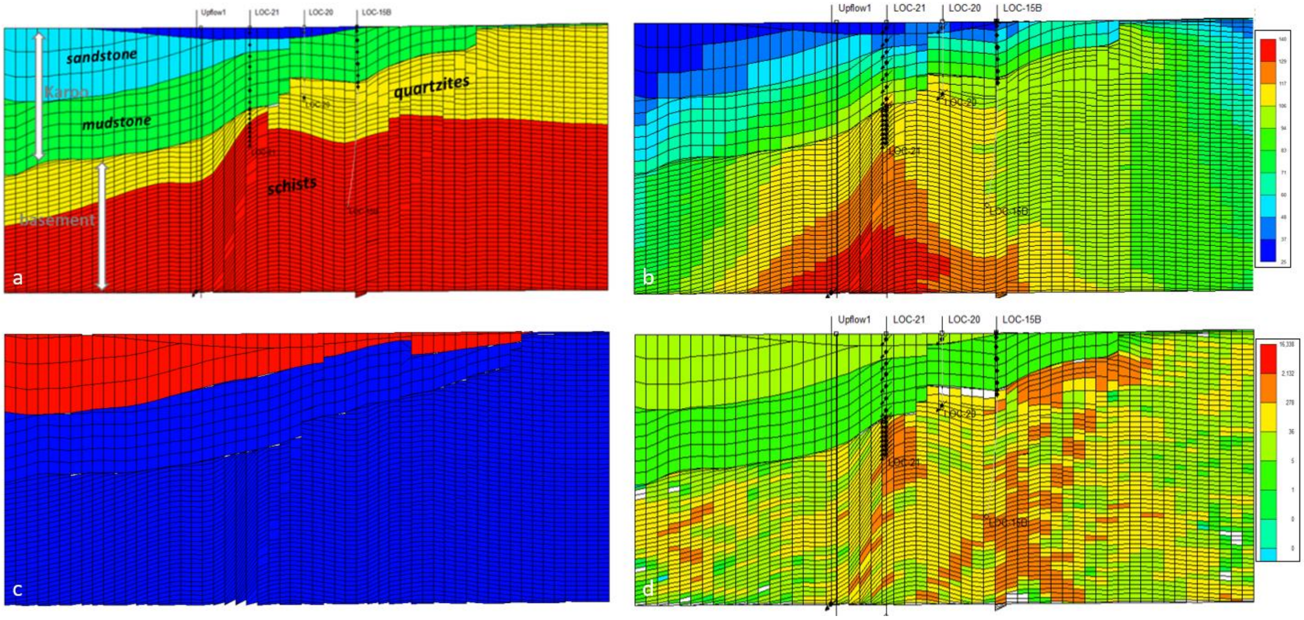

Figure 23. The zone model within the 3D simulation grid capturing a) lithology and stratigraphy units, b) temperature distribution °C, c) porosity (1% blue, 10% red), and d) DFN derived permeability distribution, mD.

5.2 Natural State Model

The dynamic model was run after initialization and the change in well temperature profiles was observed. The initial well temperatures are based on the observed/logged values in the wells and were populated in the static model. Several different parameters were modified to ensure that there is little change in well temperature profiles over time as follows:

1. Rock thermal properties: such as rock thermal conductivity and rock thermal heat capacity. Thermal conductivity was a major factor in obtaining a satisfactory match.
2. Run time: 500 years was chosen as the total equilibration period, as beyond this time the change in well temperature profiles became increasingly smaller relative to a 20 year production period.
3. Hot water inflow locations into the model: two model inflow locations were tested, which were placed based on the temperature distribution.

4. Hot water inflow rates into the model: one of the parameters that had a significant impact on well temperature profiles. It should be noted that this is also the energy being introduced into the system.
5. Aquifers: to model low temperature flow in the shallow layers (Figure 24).
6. Hot water inflow temperature and the temperature plume distribution in the model: 2 different temperature distributions were used. The temperature distribution with the higher temperatures gave a better match. This parameter also had a significant effect on wellbore temperature profiles over time.
7. Vertical permeability: in the shallower sedimentary (Karoo & Neogene) zones 1-3 (Figure 25).
8. Heat influx into the model: influx on vs off at 40 mW/m$^{2.}$

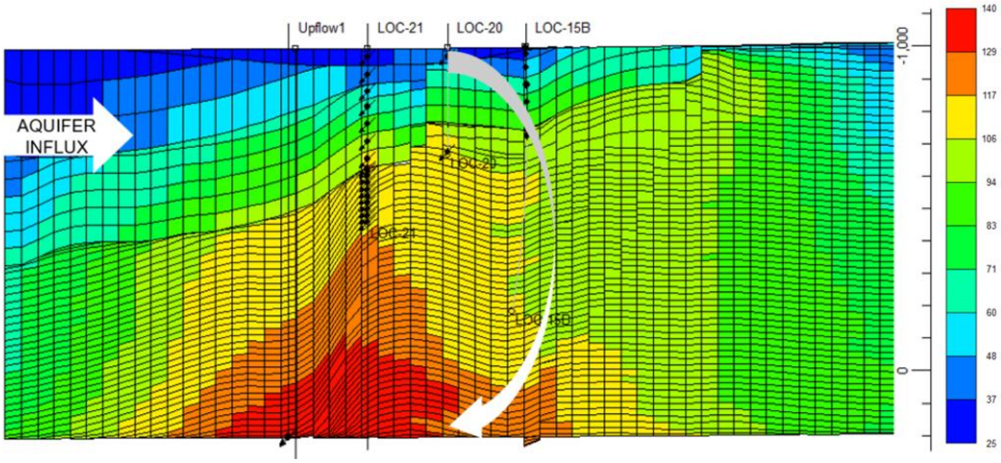

Figure 24. Temperature model in °C showing aquifer influx. The curved arrow indicates that the water influx into the model was meteoric in origin.

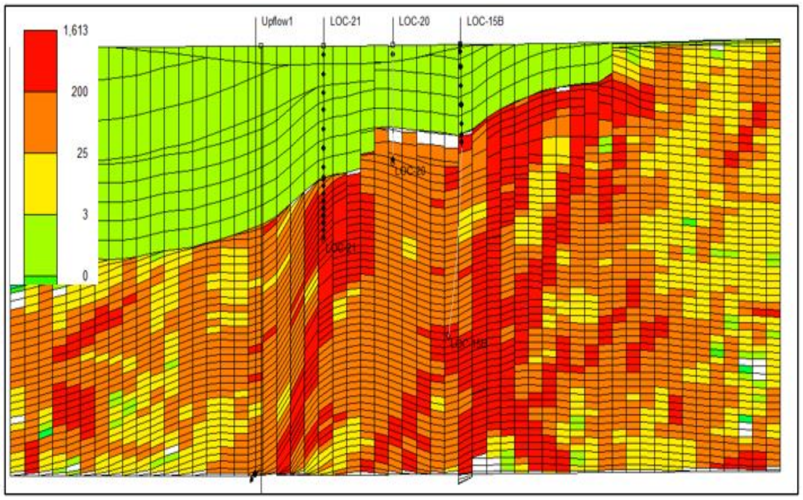

Figure 25. Log scale vertical permeability distribution, mD. The basement (zones 4 and 5 together) has higher vertical permeability due to the presence of natural fractures.

The parameters with the largest impact on achieving thermal equilibrium and matching well temperature profiles were rock thermal conductivities, temperature distribution, and inflow into the model (which also affects any thermal power potential estimates). The results of the well temperature profile matching are shown together in Figure 26.

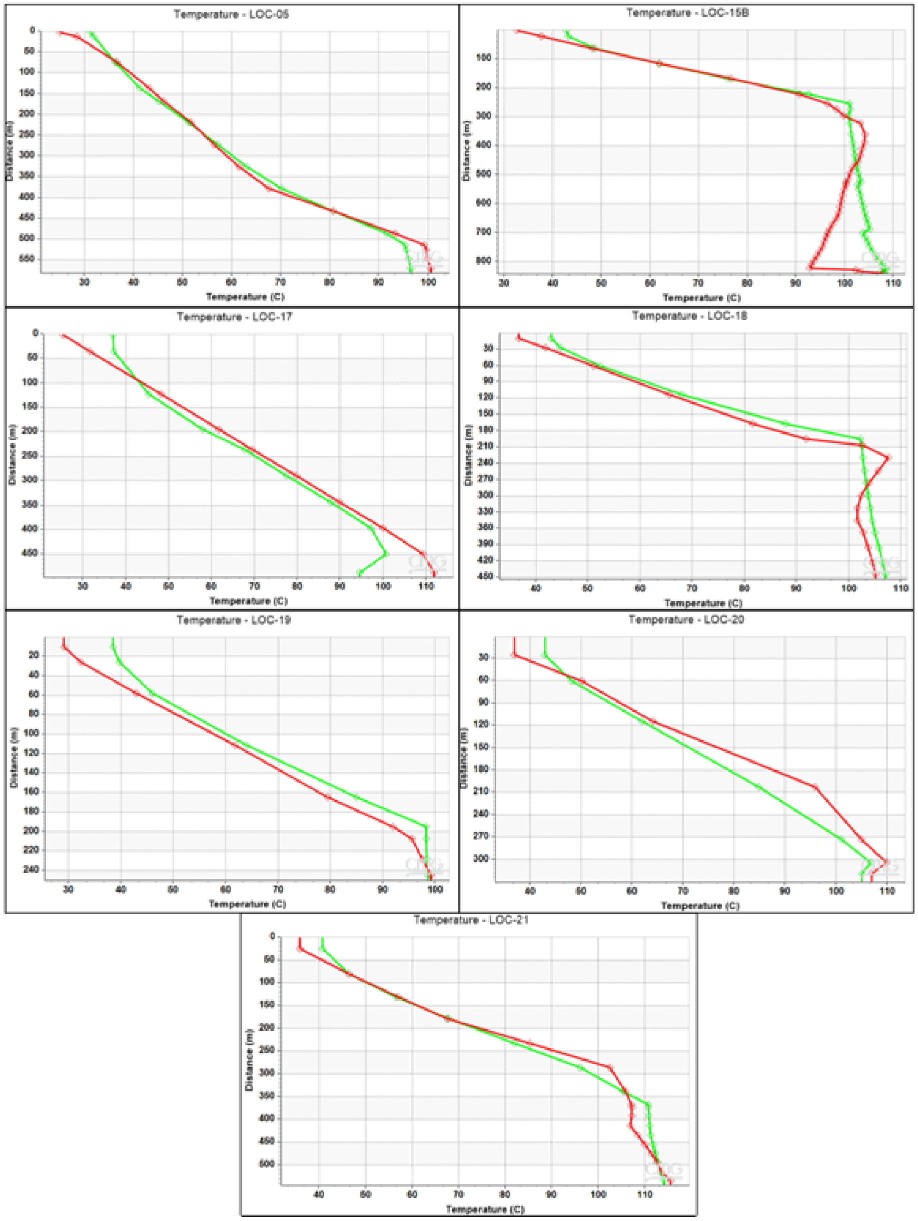

Figure 26. Well temperature profile match for all the wells. Red shows the initial well temperature profile. Green is the temperature profile after the thermal equilibrium exercise for the model.

Key observations from well temperature profile match exercise are: 1) temperature is increasing uniformly with depth through the Karoo sediments, but once within the basement the temperatures show more variable profiles due to localized hotter or cooler water inflows at different depths; 2) sharper features in temperature profiles, typically in the basement, were not matched, but overall profiles remained stable; 3) low thermal conductivity was used for the shallower, sedimentary rock zones (1-3) to blanket in the high basement temperatures and attain a good match to the mostly (except at the hot springs) near normal surface temperatures.

5.3 Production Forecasts

Several different forecast scenarios were created to estimate the geothermal power potential of the study area. The scenarios employed both existing wells, specifically LOCH-18 (which had the highest tested flow rate), LOCH-19, LOCH-20 and LOCH-21 as well as undrilled wells in conceptual development cases. The flow test results from the existing wells were used to constrain the maximum flow rate expected from the wells over the simulation. The maximum drawdown was assumed to be 3000 kPa for both injectors and producers. Injection temperature was set to 60°C. Forecasts were run for 20 years (after the 500 years for thermal equilibrium). Injection enthalpy (enthalpy at 60°C) was subtracted to calculate the net enthalpy gain in kJ/kg.

The optimal case scenario (with 3 injectors and 3 producers) produces a net thermal energy output of ~22 MWt at 25.6 kg/s with injection at 60° C. This scenario models accessing the hotter fluids that are predicted to occur at greater depth (100m below ground level) in the center of the thermal plume. Injection utilises another set of 3 new injectors (namely GGI-1, DEV5 and GGP-2) as shown in Figure 27 and 28. Production is from 3 new producers as well (namely DEV1, DEV7 and DEV21deep). DEV21deep is a deepened version (re-entry) of the LOCH-21 well with the perforations extended into the hottest temperatures in the basal layers of the plume.

These scenarios provided valuable insight to inform development strategies for the LOCH geothermal reservoir. The selection of well pairs is an important factor in optimizing the net enthalpy gain, moreover, injecting in the shallower section of the reservoir and producing from a deeper section was also seen to maximize power output. The scenario tests indicate that higher injection rates can lead to a cooling effect and hence reduce the enthalpy output over time and that energy output can be maximized by landing wells in the high temperature layers of the geothermal reservoir. The dynamic modeling provides optimized well design (insulated tubulars, length of tubing and casing, casing thickness, cement thickness etc.) to achieve maximize temperature and enthalpy output.

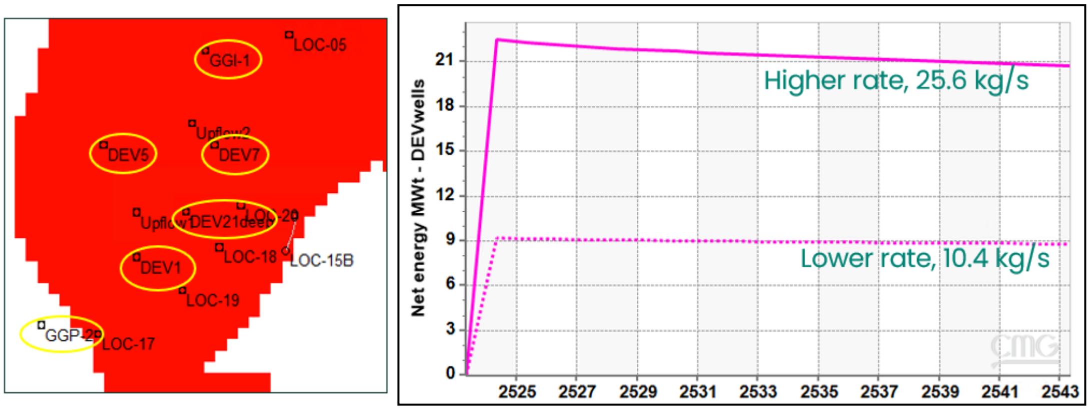

Figure 27. (Left) Well locations for optimal scenario. (Right) Net thermal power generated over time.

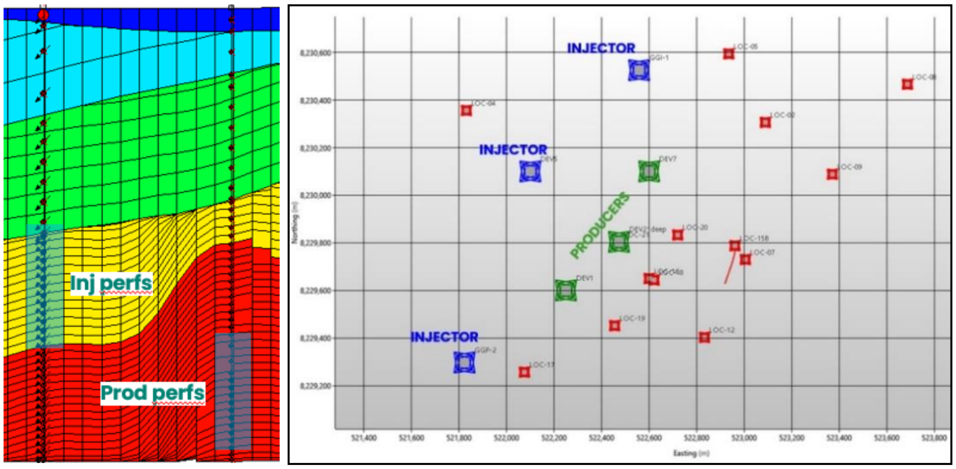

Figure 28. Well perforation arrangement and producer/injector well locations for prediction for optimal heat generation: injection perforations were at a shallower level than the production perforations to optimise the deep, hot fluid inflow.

5.4 Resource Estimation

2D mapping and the ensuing 3D modelling at the geothermal resource at Bweengwa River allows a refined characterisation of the subsurface target beyond existing flow-tested well penetrations. This study has highlighted that the revision of the existing individual temperature versus depth well log data helps to provide a more consistent areal thermal model. In addition to existing geothermometry data, the dynamic simulation (notably the model equilibration stage) gives increased verification of the presence of a hotter deep upflow supporting the tested shallow near-top basement outflow. Together these elements lead to an adjusted view of the options or strategy for further appraisal and exploitation of the resource.

The 3D geological model contains a thermal model that has equilibrated to a steady state. Filtering this model for particular isotherm values defines the area/volume of the Bweengwa resource that could be targeted for a particular temperature minimum offtake. It is not guaranteed that the rock volume has sufficient permeability to ensure offtake at all points within any particular screened volume (as flow testing to date has shown a large range in productivity) but as the fracture permeability and temperature share a dependency within the dynamic model, the occurrence of reservoir quality suitable to host development is much increased.

The top basement hosted 'shallow outflow' as tested to date and proven to deliver from 100°C (LOCH-19) up to 115°C (LOCH-21) fluid is seen to have a footprint of 2km^2 for a temperature limit of 100°C (Figure 29), but this will decrease to some 1.2km^2 filtering for a higher temperature limit of 110°C. The filtered simulation grid volume and an equivalent representative but simplified rectangular resource footprint are shown in Figure 29, with additional reference to the hosting basement rock type.

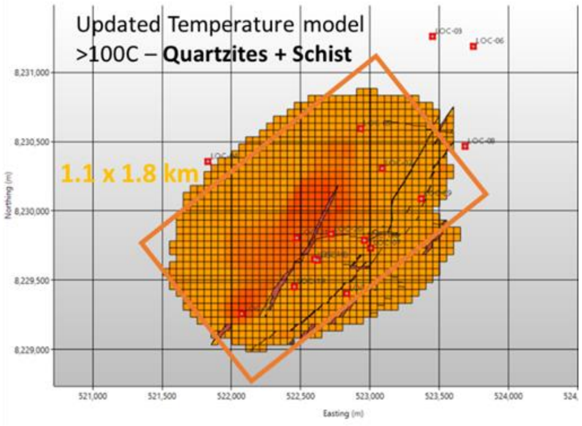

Figure 29. Simulation grid volume and an equivalent representative but simplified rectangular resource footprint of resource area for the proven shallow (top basement) geothermal resource.

6. CONCLUSIONS

This study was completed at the request of Kalahari GeoEnergy to refine the resource estimate associated with the Bweengwa River geothermal resource in the Kafue rift basin of Zambia. An initial phase of data review was found to benefit from the extensive, well organized, and sequential reporting of results obtained over the prior 10 year exploration history of this resource. Geochemical, geophysical and well derived geological datasets were considered, along with their prior integration into a previous 3D geological model. The existing model was found overall to be a suitable conceptual synthesis but noted to be lacking in its definition of the resource hosting basement.

This study has further integrated the available subsurface data to provide a realistic, possible base-case description of the targeted geothermal resource. Specific focus was placed on updating the thermal model using newly acquired deepened well data and adding characterisation of the resource hosting basement. The productivity hosting fracture system present within the basement has been modelled using a discrete fracture network (DFN) with input derived from core review and the faults contained within a newly derived fault framework. Sophisticated structural and stratigraphic geomodeling, finite element hydro-structural DFN modeling and upscaling, and advanced geothermal reservoir dynamic modeling was utilized to perform an integrated modelling workflow and deliver 3D models with predictive resource capability.

Geochemical review of sampled fluids, based on the solubility of silica and direct measurements of the same, supports that the hot water resource in most wells and springs is derived from a minimum source temperature of 130 to 140°C. The presence of a deep hot up-flow of 140 °C directly contributing to the proven 110°C resource at top basement has been included in the current model.

The integration of static parameters with the dynamic transmissivity enabled a confident initialization of the static model for simulation. Thermal equilibration runs showed stability of the thermal plume, maintaining a suitable balance of conductive and convective heat flow processes dominating in the Karoo age sedimentary cap-rock and the resource hosting metamorphic basement respectively.

The resulting 3D simulation models provide a balance between oversimplifying the subsurface and attempting to include too much, often unproven, detail. By way of example the variable response of doublet (injector-producer) scenarios that utilize existing wells captures the known variation in basement productivity.

Further flow testing of wells and especially of deepened well penetrations that will help prove the character of the assumed hotter (>130C) resource expected deeper than some 1000m below ground level. Is recommended. Accessing the hotter upflow has been simulated to deliver power output some 40% higher than proven from the shallow outflow resource tested to date.

This integration and more detailed modelling of existing data sets has advanced characterisation of the Bweengwa geothermal resource hosted in the subsurface immediately west of the Bwanda hot springs. The linkage of the Bwanda and Gwisho hot springs to the same overall deep basin circulating system is strongly supported by geochemical data, but the structural connection remains conceptual only. Further exploration potential, possibly below a deeper Karoo cover thus is envisaged in the area north of Bwanda but west of the Gwisho hot springs.

REFERENCES

Barton, C.A., Zoback, M.D.: Self-similar Distribution and Properties of macroscopic Fractures at Depth in Crystalline Rock in the Cajon Pass Scientific Drill Hole, Journal of Geophysical research, V. 97, No, B4, p5181-5200, April 10, 1992.

Davy, P.: On the frequency-length distribution of the San Andreas Fault System. Journal of Geophysical Research: Solid Earth (1978–2012), July 1993. 10.1029/93JB00372.

Edris, M.A., Haggag M., Al Benali. K., Hartley. L.J., Baxter, S, Joyce S., Shinde, A.L., Perumalla S.V., Barton, C.A.: Integrated Characterization and Modeling of Faults and Fractures: Their Impact on Reservoir Performance with Changing In-situ Stresses, Abu Dhabi. Abu Dhabi, UAE, 14–16 September 2015, SPE-175558-MS.

Geologica Geothermal Group, Inc. Geothermal Resource Assessment Report: Bweengwa River Geothermal Project. 15 October 2021.

Hale, D.: Methods to Compute Fault Images, Extract Fault Surfaces, and Estimate Fault Throws from 3D Seismic Images. Geophysics, VOL. 78, NO. 2, March-April 2013.

King, G. C. P.: The accommodation of large strains in the upper lithosphere of the Earth and other solids by self-similar fault systems: The geometrical origin of b-value, Pure Appl. Geophysics, **121**, 761–814,1983. doi:10.1007/BF02590182.

Wilmarth, M. S.: Power density update of Indonesian fields. PROCEEDINGS, The 7th Indonesia International Geothermal Convention & Exhibition (IIGCE), August 13-15, 2019, 3p.